

# A magnetic confinement nuclear fusion mechanism for solar flares

Ying-Zhi Zhang

NO.1 Nanertiao, Zhongguancun, Haidian district, Beijing, 100190 China; yzzhangmail@sohu.com

Received 20xx month day; accepted 20xx month day

**Abstract** We propose a magnetic confinement nuclear fusion mechanism for the evolution of a solar flare in solar atmosphere. The mechanism agree with two observed characteristics of explosive flares and coronal mass ejections (CMEs) that have proved to be very difficult to explain with previous mechanisms: the huge enrichments of  $^3\text{He}$  and the high energy gamma ray radiation. The twisted magnetic flux rope is a typical structure during the solar flares, which is closely related to the solar active region that magnetic fields have almost complete control over the plasma. Consequently, the plasma inside the flux rope is heated to more than  $1.0 \times 10^7$  K by adiabatic compression process, and then the thermonuclear fusion can take place in the flux rope accompanied with high energy gamma rays. We utilize the time-dependent ideal 2.5-dimensional magnetohydrodynamic (MHD) simulation to demonstrate the physical mechanism for producing flares, which reveals three stages of flare development with process of magnetic energy conversion and intense release during the solar flares and CMEs in solar atmosphere. Furthermore, we discuss the relationship between magnetic reconnection and solar eruptions.

**Key words:** Sun: flares - Sun: activity - Sun: coronal mass ejections (CMEs) - Sun: magnetic fields

## 1 INTRODUCTION

Solar flares are an intense explosion that usually occur in complex magnetic field configuration and has highly twisted magnetic flux rope structure, which are strongly associated with active region filament eruptions and coronal mass ejections (CMEs) (Jing et al. 2004, Toriumi et al. 2017). Both ground and space telescope observations show that the solar flares exhibit a variety of phenomena, which they cause electromagnetic radiations ranging from kilometric radio waves to tens of MeV gamma rays (Bastian et al. 1998, Gruber et al. 2011, Ackermann et al. 2014, Reid & Ratcliffe 2014, Benz 2017), and they produce energetic particles escaping into interplanetary space (Bai & Sturrock 1989, Hudson & Ryan 1995, Lin 2011, Reames 2013, Trottet et al. 2015, Dierckxsens et al. 2015, Cliver 2016). Specifically, a considerable puzzle is the

ciated with gamma rays burst during the solar flares (Schaeffer & Zähringer 1962, Hsieh & Simpson 1970, Kocharov & Kocharov 1984, Mason et al. 2004, Mason 2007, Nitta et al. 2015).

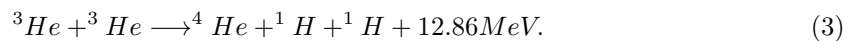
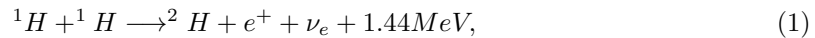
Following observational results, MHD model of the solar flares has experienced three relatively clear development stages. In the first phase, the studies have not been able to explain the time scale of a flare, which the dominant role of magnetic field in flare process has been confirmed (Hale 1908), and several important features of flare (neutral point, current sheet and magnetic reconnection, etc.) have been proposed (Giovannelli 1946, Parker 1957, Sweet 1958). In the second phase, due to the establishment of the standard flare model (Carmichael 1964, Sturrock 1966, Hirayama 1974, Kopp & Pneuman 1976), the energy storage model is the widely accepted model of a solar eruption. In the third phase, the magnetic flux rope model has been investigated extensively (Low 1996, Priest & Forbes 2002, Longcope 2005, Shibata & Magara 2011), which includes emerging magnetic flux rope model (van Tend & Kuperus 1978, Aly 1984, Forbes & Isenberg 1991, Isenberg et al. 1993, Forbes & Priest 1995, Gibson & Low 1998, Hu & Liu 2000, Chen & Shibata 2000, Lin et al. 2001, Fan 2001, Fan & Gibson 2003, Zhang et al. 2005, Zhang & Wang 2007) and shearing magnetic flux rope model (van Ballegoijen & Martens 1989, Mikic & Linker 1994, Antiochos 1998, Antiochos et al. 1999, Titov & Démoulin 1999, Amari et al. 2000, Török et al. 2004).

In fact, the physical process of making the abundant  ${}^3\text{He}$  accompanied by the high energy gamma rays usually implies the thermonuclear reaction to occur in the solar flares. Furthermore, it is critical to producing enough high temperature plasma for the thermonuclear fusion. Therefore, we propose a magnetic confinement nuclear fusion mechanism for dealing with energy conversion and intense release during the solar flares in solar atmosphere. The magnetic energy may be converted into plasma thermal energy stored in the magnetic flux rope by adiabatic compression process, and the tremendous enrichment of  ${}^3\text{He}$  and high energy gamma rays are produced by nuclear fusion during the magnetic confinement process. The purpose of this article is to discuss the details of the new mechanism for flare generation in the solar atmosphere.

## 2 THEORETICAL BASIS

### 2.1 P-p chain reaction in the sun

Hydrogen is the most abundant element in the main-sequence stars, which it can undergo thermonuclear reaction at temperature greater than  $7 \times 10^6 \text{K}$ , and p-p chain reaction is the dominant fusion reaction pattern at temperature lower than  $1.5 \times 10^7 \text{K}$  in the sun. It is now well established that the reactions making up the overwhelming bulk of the p-p chain are the following:



The rate of the reaction chain as a whole and hence the rate of energy production are controlled by the first and third reactions which take place very slowly. By contrast, the second reaction is extremely fast, effectively converting  ${}^2\text{H}$  to  ${}^3\text{He}$  only in a few seconds. At temperature  $T$  in the neighborhood of a temperature  $T_r$  (in  $1 \times 10^6 \text{K}$ ), the rate of energy production  $\epsilon$  can be expressed in the form (Salpeter 1952):

$$\rho x_H^2 \epsilon(T) \propto T^{-1} \exp\left(-\frac{E_0}{kT}\right) \quad (4)$$

where  $\rho$  is the density, and  $x_H$  is the concentrations (by mass) for hydrogen. For various temperature  $T$ , the exponent of the variation with temperature  $n$  and the rate of energy production  $\epsilon_0$  are given in Table 1 by Salpeter (1952). If the chain goes only to  ${}^3\text{He}$ , as might be the case in limited times at low temperature, then the rate of energy production in  $3 \times {}^1\text{H} \rightarrow {}^3\text{He}$  is  $\epsilon'_{pp} = 0.509x_H^{-2}\epsilon_{pp}$  (Burbidge et al. 1957).

Although we know that nuclear fusion usually occurs in the solar core, we can infer that the p-p chain reaction tend to take place during the flare process in the solar magnetic activity, for which the key ingredient in the solar flares is the anomalous overabundances of  ${}^3\text{He}$  accompanied by MeV gamma rays. The astronomical evidence suggests that nuclear reactions can take place in regions (such as stellar magnetic activity) on the stellar surface, for which the regions develop sufficient magnetic energy to accelerate particles (Fowler et al. 1955). We conclude that the plasma can be heated to much more than  $7.0 \times 10^6\text{K}$  by a magnetic confinement mechanism in the solar active region, and then  ${}^3\text{He}$  is the end product of nuclear reaction since solar flares have lasted only a few hours in the solar atmosphere. Under astrophysical conditions, we assume that the equation used to calculate the rate of energy production of nuclear reaction at the interior of the sun is also applicable to calculate that at the solar surface. Then for temperature  $T_f$  and density  $\rho_f$  in the core of solar flares, the rate of energy production  $\epsilon_f$  in the flare process can be expressed in the form:

$$\epsilon_f = 2.545 \times 10^{-25} \rho_f T_f^4 \text{erg} \cdot \text{g}^{-1} \cdot \text{s}^{-1} \cdot \text{K}^{-4}. \quad (5)$$

## 2.2 Magnetic confinement in the solar atmosphere

Due to the higher conductivity in the solar atmosphere, ideal MHD method is suitable for studying the evolution of the solar flare events. Furthermore, magnetic flux emergence from the solar photosphere into the corona is the driver of a variety of phenomena and the inclusion of different physical effects (such as magnetic flux rope formation, current sheet, and magnetic reconnection) associated with solar activity (Cheung & Isobe 2014). We consider that the magnetic flux rope suspended in the corona with a transverse current sheet above and a vertical current sheet below may be the magnetic confinement structure in solar atmosphere.

The solar flares start with a magnetic flux rope formatted by magnetic emergence. The plasma inside the twisted magnetic flux rope is adiabatically heated by the helical magnetic field. We conclude that some of the magnetic energy is converted into plasma thermal energy by adiabatic compression and the remainder of the magnetic energy has strengthened the magnetic flux rope structure during the process of the magnetic confinement. For completely ionized plasma in the corona, suppose ions and electrons inside the flux rope are at the same temperature (named plasma temperature). While the temperature of the pinched plasma is greater than  $7 \times 10^6\text{K}$ , the thermonuclear fusion can take place in the magnetic flux rope.

Finally, the magnetic confinement structure is destroyed by magnetic reconnection. While current density of vertical current sheet reaches its peak value, the magnetic reconnection may occur in the current sheet associated with nuclear explosion, which is similar to the phenomenon of short circuit in conductors. The magnetic reconnection is a key ingredient of many astrophysical phenomena, which the release of stored magnetic energy is facilitated by the ideal MHD process (Pontin 2012). Furthermore, free magnetic

connection. Specifically, because of thermonuclear reactions, particles get kinetic energy not by some kinds of acceleration mechanism, but by high temperature.

### 3 NUMERICAL MODEL

We utilize time-dependent ideal 2.5-dimensional MHD simulation of the two-stage catastrophic magnetic flux rope model to illustrate the evolution of the solar flares (Zhang 2013, 2015). In spherical coordinates  $(r, \theta, \varphi)$ , a magnetic flux function  $\psi(t, r, \theta)$  was presented, and it has to do with magnetic field by

$$\mathbf{B} = \nabla \times \left( \frac{\psi}{r \sin \theta} \hat{\varphi} \right) + \mathbf{B}_\varphi, \quad \mathbf{B}_\varphi = B_\varphi \hat{\varphi}, \quad (6)$$

where  $B_\varphi$  is the azimuthal component of the magnetic field. The ideal MHD equations are the following form:

$$\frac{\partial \rho}{\partial t} + \nabla \cdot (\rho \mathbf{v}) = 0, \quad (7)$$

$$\begin{aligned} \frac{\partial \mathbf{v}}{\partial t} + \mathbf{v} \cdot \nabla \mathbf{v} + \frac{1}{\rho} \nabla p + \frac{1}{\mu \rho} [L\psi \nabla \psi + \mathbf{B}_\varphi \times (\nabla \times \mathbf{B}_\varphi)] \\ + \frac{1}{\mu \rho r \sin \theta} \nabla \psi \cdot (\nabla \times \mathbf{B}_\varphi) \hat{\varphi} + \frac{GM_\odot}{r^2} \hat{r} = 0, \end{aligned} \quad (8)$$

$$\frac{\partial \psi}{\partial t} + \mathbf{v} \cdot \nabla \psi = 0, \quad (9)$$

$$\frac{\partial B_\varphi}{\partial t} + r \sin \theta \nabla \cdot \left( \frac{B_\varphi \mathbf{v}}{r \sin \theta} \right) + \left[ \nabla \psi \times \nabla \left( \frac{v_\varphi}{r \sin \theta} \right) \right]_\varphi = 0, \quad (10)$$

$$\frac{\partial T}{\partial t} + \mathbf{v} \cdot \nabla T + (\gamma - 1) T \nabla \cdot \mathbf{v} = 0, \quad (11)$$

where

$$L\psi \equiv \frac{1}{r^2 \sin^2 \theta} \left( \frac{\partial^2 \psi}{\partial r^2} + \frac{1}{r^2} \frac{\partial^2 \psi}{\partial \theta^2} - \frac{\cot \theta}{r^2} \frac{\partial \psi}{\partial \theta} \right), \quad (12)$$

For an ideal adiabatic compression process, the polytropic index is  $\gamma = 2.3$ . The solution domain is  $1 \leq r \leq 30$ ,  $0 \leq \theta \leq \pi/2$ . It is discretized into  $130 \times 90$  grid points. The above MHD equations are solved with the multi-step implicit scheme developed by Hu (1989).

In this study, we choose the essential physical parameters of bottom of the corona above the active region, which the temperature  $T_0 = 3 \times 10^6$  K and the density  $\rho_0 = 1.67 \times 10^{-11} \text{ kg} \cdot \text{m}^{-3}$ . In the following, the solar radius  $R_s$  is the unit of length, and the ration of gas pressure to magnetic pressure is  $\beta = 0.01$ , so that the unit of  $\psi$  is  $\psi_0 = (2\mu\rho_0 R T_0 R_s^4 / \beta)^{1/2} = 6.97 \times 10^{15} \text{ Wb}$ , and the unit of magnetic field intensity is  $B_0 = \psi_0 / R_s^2 = 1.44 \times 10^{-2} \text{ T}$ . Some other units of interest are  $E_0 = B_0^2 R_s^3 / \mu = 5.563 \times 10^{28} \text{ J}$  for magnetic energy,  $v_A = B_0 / (\mu \rho_0)^{1/2} = 3150 \text{ km} \cdot \text{s}^{-1}$  for velocity,  $\tau_A = R_s / v_A = 220 \text{ s}$  for time, and  $j_0 = B_0 / (\mu R_s) = 1.65 \times 10^{-5} \text{ A} \cdot \text{m}^{-2}$  for current density.

A quadrupole field is chosen for the initial background magnetic field (see Fig. 3a). The related magnetic flux function normalized by  $\psi_0$  is given by

$$\psi(r, \theta) = \frac{\sin^2 \theta}{r} + \frac{(3 + 5 \cos 2\theta) \sin^2 \theta}{2r^3}, \quad (13)$$

where  $r$  is in the unit of  $R_s$ . During the evolution of the magnetic flux rope system, two stage catastro-

macroscopic instability, and the magnetic reconnection occurs in the vertical current sheet while the current density gets the maximum value.

The magnetic energy ( $E$ ) of the force-free magnetic field is normalized by  $4\pi E_0$ , and calculated by the following equation:

$$E = \frac{1}{2} \int_1^{30} dr \int_0^{\pi/2} B^2 r^2 \sin \theta d\theta + \frac{30^3}{2} \int_0^{\pi/2} (B_r^2 - B_\theta^2)_{r=30} \sin \theta d\theta, \quad (14)$$

where the first term on the right is the magnetic energy in the computational domain ( $1 \leq r \leq 30$ ;  $0 \leq \theta \leq \pi$ ;  $0 \leq \varphi \leq 2\pi$ ) and the second is outside the domain (see Hu 2004). The magnetic energy is  $E_p = 1.476$  for the initial quadrupolar potential field, and  $E_m = 1.662$  for the corresponding partly open field (see Zhang et al. 2005). Moreover, the magnetic energy inside the flux rope ( $E_r$ ) is calculated by the representation similar to the first term on the right of the equation (14), but with the integral domain limited to the interior of the flux rope.

## 4 NUMERICAL RESULT

In our simulation, the magnetic flux rope is described with its toroidal magnetic flux ( $\Phi_p$ ) and poloidal flux ( $\Phi_\varphi$ ), which are deterministic throughout the magnetic flux emergence in the evolution of the magnetic flux rope system. In present study, the initial condition is in an equilibrium state,  $\Phi_p = 0.42$  and  $\Phi_\varphi = 0.0544$ . Base on the result, we illustrate the key characteristics of flare development, such as magnetic flux rope for the formation of magnetic confinement structure, high temperature plasma for thermonuclear fusion and magnetic reconnection associated with nuclear explosion in the corona. Furthermore, the two stage catastrophes are the mechanism driving the eruption of magnetic flux rope in the simulation.

### 4.1 Formation of the magnetic confinement structure

Two parameters are used to describe the geometrical characteristics of the flux rope system in equilibrium. One is the height of the flux rope axis,  $h_a$ , and the other is the length of the vertical current sheet,  $h_c$ . Figure 1 shows that there are two stages of catastrophes during the evolution of the magnetic flux rope system in the solar corona, and the flux rope has maintained a certain period of relative stability between the two catastrophes. The magnetic flux rope has emerged from the photosphere into the solar corona after  $1\tau_A$ . Then the first catastrophe occurs in the flux rope system at  $4\tau_A$ , which the vertical current sheet appears below the flux rope. At  $39\tau_A$ , the second catastrophe occurs with the flux rope escaping.

As seen from Figure 2, the plasma temperature at the flux rope axis,  $T_a$ , and the plasma density at the flux rope axis,  $\rho_a$ , are represented during the flare evolution in the solar corona, respectively. Since the plasma is subjected to adiabatic compression by the magnetic field,  $T_a$  has been greater than  $1 \times 10^7$  K from  $1\tau_A$  to  $41\tau_A$  (Fig. 2a). At the early stage of magnetic flux rope eruption, a hot channel with a temperature as high as  $1 \times 10^7$  K along the magnetic flux rope was found by SDO/AIA observations (see Zhang et al. 2012). This numerical result may explain the observations. While the flux rope just emerges into the solar corona at  $1\tau_A$ ,  $T_a$  reaches its maximum value,  $3.494 \times 10^7$  K (see Fig. 3b). We conclude that the plasma can be ignited and thermonuclear reaction takes place inside the flux rope because this temperature ( $3.494 \times 10^7$

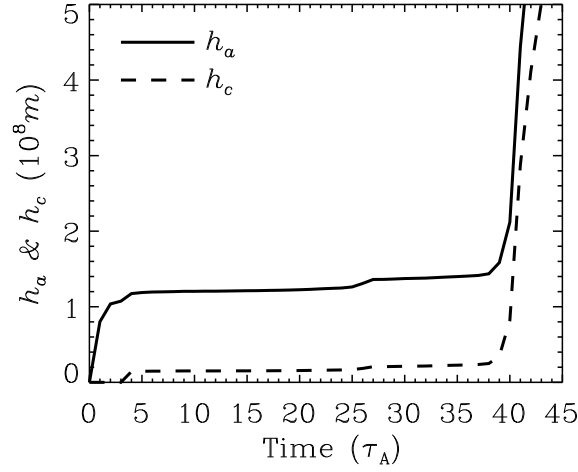


Fig. 1: Height of the flux rope axis,  $h_a$  vs. time (solid lines), and height of the vertical current sheet under the flux rope,  $h_c$  vs. time (dashed lines).

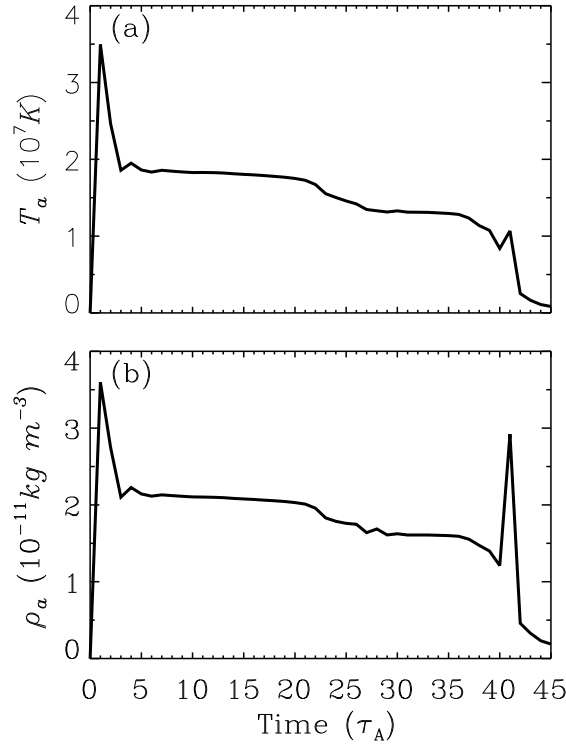


Fig. 2: Plasma temperature at the flux rope axis,  $T_a$  vs. time (a), and plasma density at the flux rope axis,  $\rho_a$  vs. time (b).

at  $3\tau_A$ , and drops from  $1.950 \times 10^7$  K to  $1.067 \times 10^6$  K until the eruption at  $41\tau_A$ . During the evolution of the flux rope system,  $\rho_a$  has remained at about  $2.0 \times 10^{-11} \text{ kg} \cdot \text{m}^{-3}$  except before the first catastrophe and after the second catastrophe (Fig. 2b).

Furthermore, after the first catastrophe occurs in the magnetic flux rope system, a vertical current sheet is formed below the flux rope, and a curved transverse current sheet developed from a neutral point is formed above the flux rope, which the high temperature region appears near the two footpoints of the transverse current sheet (about  $8 \times 10^6$  K) and inside the magnetic flux rope (greater than  $1 \times 10^7$  K), respectively (see

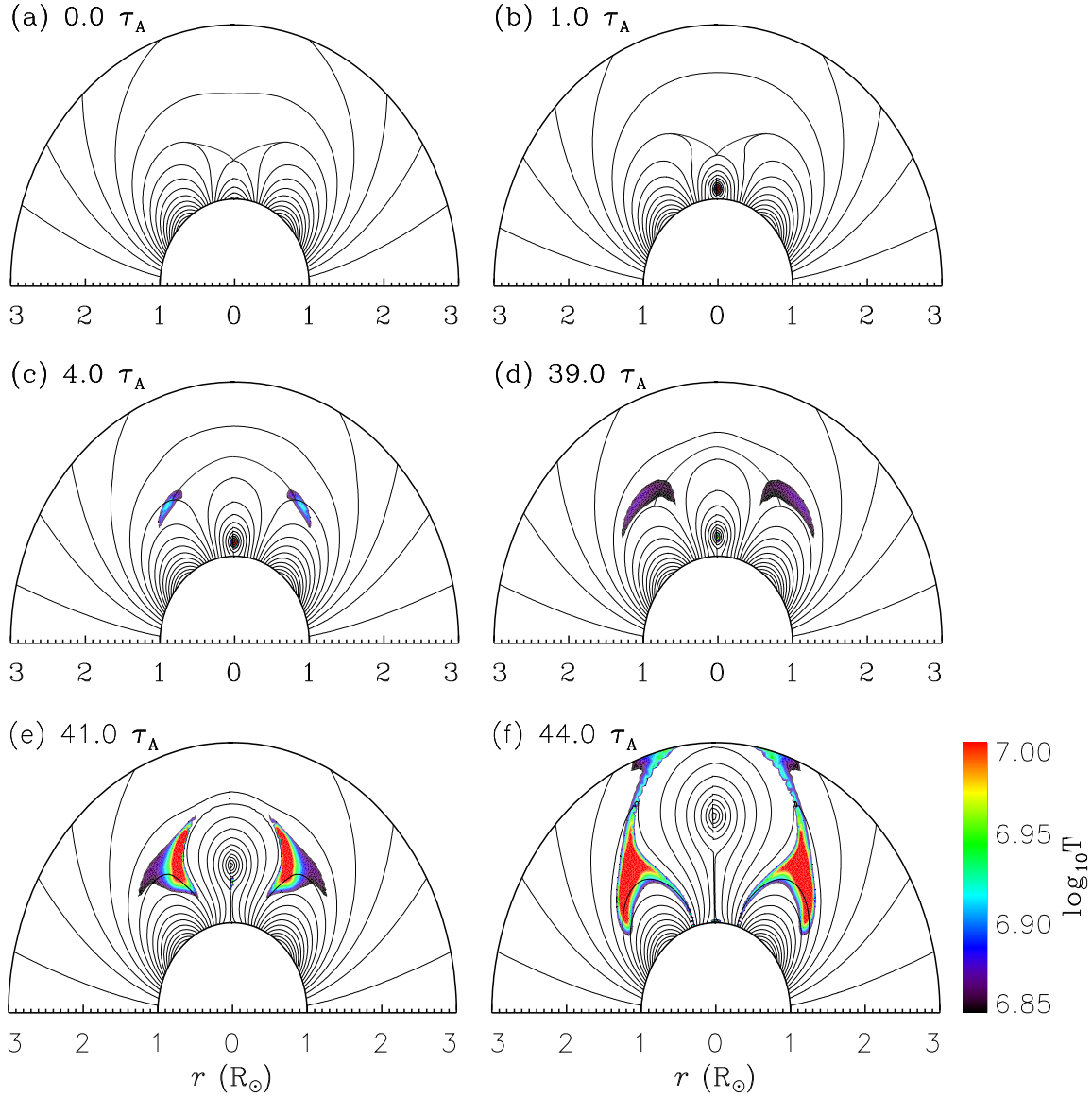


Fig. 3: In order to show topology of the magnetic field and explosive flares clearly, magnetic configuration (black contours) and temperature distribution (color scale) are shown at six separate time, which are the initial quadrupole magnetic field (a), the flux rope just emerging into the solar corona (b), the start of the solar flares just after the first catastrophe (c), the end of the pre-flare just before the second catastrophe (d), magnetic reconnection just occurring in the vertical current sheet (e) and the end of the solar flares (f). The dark blue and bright red correspond to  $7.08 \times 10^6$  and  $1.0 \times 10^7$  K, respectively.

with two current sheets has been formed in the corona after the first catastrophe, which the high temperature plasma heated by an adiabatic compression process in the twisted magnetic flux rope is involved in the thermonuclear fusion reaction.

#### 4.2 Evolution of the solar flares

Figure 4 shows that there are three different trends in the variation of current density in the vertical current sheet. Accordingly, we believe that the solar flares usually consist of three stages: pre-flare phase ( $4-39\tau_A$ ),

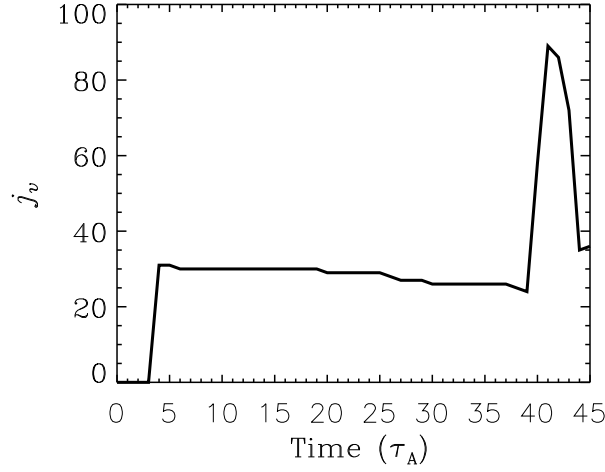


Fig. 4: Current density of the vertical current sheet,  $j_v$  vs. time, the unit of  $j_v$  is  $j_0 = 1.65 \times 10^{-5} \text{ A} \cdot \text{m}^{-2}$ .

taken place slowly and steadily inside the flux rope, for which  $T_a$  has been much higher than  $7 \times 10^6$  K for about 2.14 hours. Meanwhile, magnetic pinch process has maintained the plasma temperature to keep the reaction going on. As a result, a large number of  $^2\text{H}$  and  $^3\text{He}$  accompanied by high energy gamma rays have been produced in the former two steps of the p-p chain, which the duration of the pre-flare phase often determines production of  $^3\text{He}$ .

Subsequently, second catastrophe occurs just after  $39\tau_A$ , at which the vertical current sheet starts to stretch rapidly upwards, and then its current density increases rapidly and gets the maximum value at  $41\tau_A$  (Fig. 4). Due to magnetic flux rope upward movement, plasma temperature inside the flux rope has been lowered, and the high temperature zone has expanded at the footpoint on either side of the transverse current sheet (see Fig. 3d). The violent nuclear explosion in the flux rope is triggered by the second catastrophe, and magnetic reconnection occurs in the vertical current sheet while current density reaches its maximum at  $41\tau_A$ . In the meantime, magnetic reconnection in the transverse current sheet produces two high temperature banding area (above  $1 \times 10^7$  K), for which a large number of accelerated charged particles bombard the lower atmosphere along magnetic field lines (see Fig. 3e). We further conclude that the flare phase begins with the second catastrophe and ends with magnetic reconnection in the vertical current sheet.

While current density of the vertical current sheet reduces quickly and returns to vicinity of the value before the second catastrophe, the transverse current sheet fully reconnects and magnetic flux rope bursts out (CMEs) at  $44\tau_A$  (see Fig. 3f). There are two large high temperature areas at both footpoints (greater than  $1 \times 10^7$  K), which are the double hard X-ray sources. In the post-flare phase, CMEs are triggered by magnetic reconnection in both vertical and transverse current sheets, and high temperature products (such as high-energy  $^1\text{H}$ ,  $^2\text{H}$  and  $^3\text{He}$ ) generated by the nuclear fusion reaction inside the flux rope are ejected from corona into interplanetary space, simultaneously. However, plasma macroscopic stability is a prerequisite to the solar flares during evolution of magnetic flux rope system.

#### 4.3 Energy conversion in the solar flares

Solar flares are high energy astrophysical events that occur frequently in the solar atmosphere accompanied



Table 1: Calculated magnetic flux rope system parameters at different times.

$\tau_A$	$T_a$ ( $10^6 \text{ K}$ )	$\rho_a$ ( $10^{-11} \text{ kg} \cdot \text{m}^{-3}$ )	$n_a$ ( $10^{16} \text{ m}^{-3}$ )	$R_a$ ( $10^8 \text{ m}$ )	$E_H$ ( $10^{-16} \text{ J}$ )	$E$ ( $E_0=5.563 \times 10^{28} \text{ J}$ )	$E_r$ ( $E_0$ )
0	3	1.67	1	0	1.036	1.476	0
1	34.94	3.597	2.154	0.802	12.06	1.730	0.1854
41	10.67	2.921	1.749	1.564	3.683	1.707	0.1143

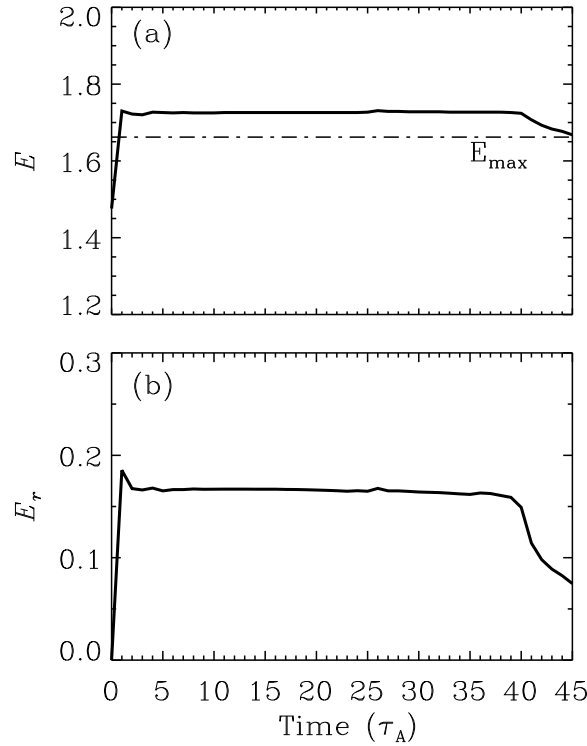


Fig. 5: Magnetic energy of the system,  $E$  vs. time (a), that of the flux rope,  $E_r$  vs. time (b), and unit of the magnetic energy is  $E_0 = 5.563 \times 10^{28} \text{ J}$ .

the details of the energy conversion during the solar flare process given in Table 1, which magnetic energy is converted into thermal energy, and hydrogen burns to release nuclear energy, at last, some of the remaining magnetic energy drives coronal mass ejections into space.

As magnetic flux emerges into the solar corona, the magnetic flux rope system gains magnetic energy. About  $1.413 \times 10^{28} \text{ J}$  of the added magnetic energy is used to maintain balance of the flux rope system, that is why the magnetic confinement structure remains  $40\tau_A$  in the corona. Besides, about  $5.390 \times 10^{25} \text{ J}$  magnetic energy is converted into thermal energy of the plasma inside the flux rope by an adiabatic compression process at about  $1\tau_A$ . Thus plasma inside the flux rope has been heated to  $3.494 \times 10^7 \text{ K}$ , which  $^1\text{H}$  has obtained very high average kinetic energy, and then burns in the flux rope of radius  $0.802 \times 10^8 \text{ m}$ . We assume that is the core region of magnetic field heating plasma in the flux rope.

For values of mean temperature  $T_f = 1.625 \times 10^7 \text{ K}$  and mean density  $\rho_f = 1.950 \times 10^{-11} \text{ kg} \cdot \text{m}^{-3}$  in core of the flux rope during process of thermonuclear fusion, we use the above equation (5) to calculate the

with very low fusion rate, the amount of nuclear energy produced also depends on both the timing of the fusion and the size of the fusion region ( $m^{-3}$ ). Thus, from  $1\tau_A$  to  $41\tau_A$ , the total amount of nuclear energy produced in the flux rope is estimated at about  $3.045 \times 10^{-7} \text{J} \cdot m^{-3}$ . Furthermore, we can estimate that about  $2.746 \times 10^5 (m^{-3})$   ${}^3\text{He}$  are produced during the solar flares. For different sizes of nuclear reaction regions ( $m^3$ ), we can calculate the nuclear energy produced and the amount of  ${}^3\text{He}$ . This seems to suggest that the solar flares maybe a magnetic confinement fusion process, in which thermonuclear reaction of hydrogen is enough to produce up to a factor of ten thousand of  ${}^3\text{He}$  even in the extremely low rate of energy production for several hours in the solar magnetic active region. Obviously, the thermonuclear fusion produces not only  ${}^3\text{He}$  but also high energy gamma rays that is used to be a considerable puzzle observational phenomenon.

Figure 5 shows that magnetic energy of the flux rope system,  $E$ , and energy of the flux rope,  $E_r$ , as a function of time, have the similar trend. A dot-dashed line in Figure 5a denotes the corresponding partly open field energy  $E_m=1.662$ . It should be noted that the magnetic energy remains stably until  $41\tau_A$ , which magnetic reconnection occurs in the vertical current sheet and triggers the CMEs. While the transverse current sheet fully reconnects at about  $44\tau_A$ , magnetic energy of the system drops from 1.707 to 1.677. Meanwhile about  $8.345 \times 10^{26} \text{J}$  of magnetic energy in the system is released suddenly, and the magnetic flux rope is thrown out with massive high energy particles (CMEs).

## 5 CONCLUSIONS

Our result suggests that the solar flares usually represented in three phases (pre-flare, flare and post-flare) may be a process of magnetic confinement nuclear fusion in solar atmosphere. After the first catastrophe, the magnetic confinement structure appears in the form of a magnetic flux rope with a vertical current sheet below and a transverse current sheet above. Between the first and second catastrophe (pre-flare phase), the plasma heated by adiabatic compression process in the flux rope has been involved in the steady thermonuclear fusion. From the second catastrophe to magnetic reconnection just in the vertical current sheet (flare phase), the solar flares manifest the process of the transient nuclear explosion accompanied by high energy gamma rays. While magnetic reconnection occurs in both the vertical and the transverse current sheets (post-flare phase), thermonuclear fusion products (including  ${}^3\text{He}$  and other high energy particles) with magnetic flux rope and plasma in the corona are injected into interplanetary space, simultaneously (CMEs).

We conclude that the solar flares are probably resulted from loss of equilibrium in the complex magnetic configurations, and produced by magnetic confinement nuclear fusion of the plasma during the ideal MHD process in solar atmosphere. Magnetic reconnection is a key element of the solar flares, which occurs in an impulsive way in the solar corona. Furthermore, magnetic reconnection may be a general phenomenon closely coincided with the nuclear fusion explosion, and triggers the CMEs without plasma macroscopic instability. In addition, the high energy particles involved in the solar flare process maybe accelerate not by some kinds of acceleration mechanism, but by high temperature.

**Acknowledgements** The authors are greatly indebted to the anonymous referee for helpful comments and

## References

- Ackermann, M., Ajello, M., Albert, A., et al., 2014, *ApJ*, 787, 15
- Aly, J. J., 1984, *ApJ*, 283, 349
- Amari, T., Luciani, J. F., Mikic, Z., Linker, J., 2000, *ApJ*, 529, L49
- Antiochos, S. K., 1998, *ApJ*, 502, L181
- Antiochos, S. K., Devore, C. R., Klimchuk, J. A., 1999, *ApJ*, 510, 485
- Bai, T., Sturrock, P. A., 1989, *ARA&A*, 27, 421
- Bastian, T. S., Benz, A. O., Gary, D. E., 1998, *ARA&A*, 36, 1
- Benz, A. O., 2017, *LRSP*, 14, 2
- Burbidge, E. M., Burbidge, G. R., Fowler, W. A., Hoyle, F., 1957, *RvMP*, 29, 547
- Carmichael, H., 1964, *NASSP*, 50, 451
- Chen, P. F., Shibata, K., 2000, *ApJ*, 545, 524
- Cheung, M. C. M., Isobe, H., 2014, *LRSP*, 11, 3
- Cliwer, E. W., 2016, *ApJ*, 832, 128
- Dierckxsens, M., Tziotziou, K., Dalla, S., et al., 2015, *SoPh*, 290, 841
- Fan, Y., 2001, *ApJ*, 554, L111
- Fan, Y., Gibson, S. E., 2003, *ApJ*, 589, L105
- Forbes, T. G., Isenberg, P. A., 1991, *ApJ*, 373, 294
- Forbes, T. G., Priest, E. R., 1995, *ApJ*, 446, 377
- Fowler, W. A., Burbidge, G. R., Burbidge, E. M., 1955, *ApJS*, 2, 167
- Gibson, S. E., Low, B. C., 1998, *ApJ*, 493, 460
- Giovanelli, R. G., 1946, *Natur*, 158, 81
- Gruber, D., Lachowicz, P., Bissaldi, E., et al., 2011, *A&A*, 533, A61
- Hale, G. E., 1908, *ApJ*, 28, 315
- Hirayama, T., 1974, *SoPh*, 34, 323
- Hsieh, K. C., Simpson, J. A., 1970, *ApJ*, 162, L191
- Hu, Y. Q., 1989, *J. Comput. Phys.*, 84, 441
- Hu, Y. Q., 2004, *ApJ*, 607, 1032
- Hu, Y. Q., Liu, W., 2000, *ApJ*, 540, 1119
- Hudson, H., Ryan, J., 1995, *ARA&A*, 33, 239
- Isenberg, P. A., Forbes, T. G., Demoulin, P., 1993, *ApJ*, 417, 368
- Jing, J., Yurchyshyn, V. B., Yang, G., Xu, Y., Wang, H., 2004, *ApJ*, 614, 1054
- Kocharov, L. G., Kocharov, G. E., 1984, *SSRv*, 38, 89
- Kopp, R. A., Pneuman, G. W., 1976, *SoPh*, 50, 85
- Lin, J., Forbes, T. G., Isenberg, P. A., 2001, *JGR*, 106, 25053
- Lin, R. P., 2011, *SSRv*, 159, 421
- Longcope, D. W., 2005, *LRSP*, 2, 7
- Low, B. C., 1996, *SoPh*, 167, 217
- Mason, G. M., Mazur, J. E., Dwyer, J. R., et al., 2004, *ApJ*, 606, 555

- Mason, G. M., 2007, SSRv, 130, 231
- Mikic, Z., Linker, J. A., 1994, ApJ, 430, 898
- Nitta, N. V., Mason, G. M., Wang, L. H., Cohen, C. M. S., Wiedenbeck, M. E., 2015, ApJ, 806, 235
- Parker, E. N., 1957, JGR, 62, 509
- Pontin, D. I., 2012, PTRSA, 370, 3169
- Priest, E. R., Forbes, T. G., 2002, A&ARv, 10, 313
- Reames, D. V., 2013, SSRv, 175, 53
- Reid, H. A. S., Ratcliffe, H., 2014, RAA, 14, 773
- Salpeter, E. E., 1952, ApJ, 116, 649
- Schaeffer, O. A., Zähringer, J., 1962, PhRvL, 8, 389
- Shibata, K., Magara, T., 2011, LRSP, 8, 6
- Sturrock, P. A., 1966, Natur, 211, 695
- Sweet, P. A., 1958, IAU Sym., 6, 123
- Titov, V. S., Démoulin, P., 1999, A&A, 351, 707
- Toriumi, S., Schrijver, C. J., Harra, L. K., Hudson, H., Nagashima, K., 2017, ApJ, 834, 56
- Török, T., Kliem, B., Titov, V. S., 2004, A&A, 413, L27
- Trottet, G., Samwel, S., Klein, K. L., Dudok de Wit, T., Miteva, R., 2015, SoPh, 290, 819
- van Ballegooijen, A. A., Martens, P. C. H., 1989, ApJ, 343, 971
- van Tend, W., Kuperus, M., 1978, SoPh, 59, 115
- Zhang, J., Cheng, X., Ding, M. D., 2012, NatCo, 3, 747
- Zhang, Y. Z., 2013, ApJ, 777, 52
- Zhang, Y. Z., 2015, ApJ, 800, 43
- Zhang, Y. Z., Hu, Y. Q., Wang, J. X., 2005, ApJ, 626, 1096
- Zhang, Y. Z., Wang, J. X., 2007, ApJ, 663, 592